Journal of Biomechanics 49 (2016) 3901–3907

Contents lists available at ScienceDirect

Journal of Biomechanics

journal homepage: www.elsevier.com/locate/jbiomech
www.JBiomech.com

Lumped-parameter electromyogram-driven musculoskeletal hand model: A potential platform for real-time prosthesis control

Dustin L. Crouch *, He Huang

UNC-NC State Joint Department of Biomedical Engineering, North Carolina State University, Raleigh, NC 27695, USA

ARTICLE INFO

Article history:
Accepted 21 October 2016

Keywords:
Wrist
Simulation
Amputation
Parameter
Optimization

ABSTRACT

Simple, lumped-parameter musculoskeletal models may be more adaptable and practical for clinical real-time control applications, such as prosthesis control. In this study, we determined whether a lumped-parameter, EMG-driven musculoskeletal model with four muscles could predict wrist and metacarpophalangeal (MCP) joint flexion/extension. Forearm EMG signals and joint kinematics were collected simultaneously from 5 able-bodied (AB) subjects. For one subject with unilateral transradial amputation (TRA), joint kinematics were collected from the sound arm during bilateral mirrored motion. Twenty-two model parameters were optimized such that joint kinematics predicted by EMG-driven forward dynamic simulation closely matched measured kinematics. Cross validation was employed to evaluate the model kinematic predictions using Pearson's correlation coefficient (r). Model predictions of joint angles were highly to very highly positively correlated with measured values at the wrist (AB mean $r=0.94$, TRA $r=0.92$) and MCP (AB mean $r=0.88$, TRA $r=0.93$) joints during single-joint wrist and MCP movements, respectively. In simultaneous multi-joint movement, the prediction accuracy for TRA at the MCP joint decreased ($r=0.56$), while r-values derived from AB subjects and TRA wrist motion were still above 0.75. Though parameters were optimized to match experimental sub-maximal kinematics, passive and maximum isometric joint moments predicted by the model were comparable to reported experimental measures. Our results showed the promise of a lumped-parameter musculoskeletal model for hand/wrist kinematic estimation. Therefore, the model might be useful for EMG control of powered upper limb prostheses, but more work is needed to demonstrate its online performance.

1. Introduction

Computational musculoskeletal models have been used extensively to investigate healthy and impaired human movement (Higginson et al., 2006; Zajac et al., 2002) and simulate surgery and rehabilitation (Delp et al., 1990; Saul et al., 2003; Shelburne and Pandy, 1998), among other applications. Forward dynamic simulation, when applied to musculoskeletal models, can generate joint kinematic predictions from input electromyogram (EMG) signals. Forward dynamic simulation has primarily been used offline, for example, to estimate muscular biomechanical contributions to movement (Neptune et al., 2001) and joint loading (Manal and Buchanan, 2013). When executed in real-time, forward dynamic simulation could generate motion predictions for external devices, such as powered prostheses (Eilenberg et al., 2010).

Many upper limb musculoskeletal models implemented for real-time EMG-driven forward dynamic simulation include numerous musculoskeletal elements to accurately represent anatomy and generate physiologic predictions. Model complexity has ranged from 5 muscles and 1 degree of freedom (DOF) to predict isometric elbow joint moments (Manal et al., 2002), to 138 muscles and 11 DOFs to investigate the complex motions of the arm and shoulder girdle (Chadwick et al., 2009). Unfortunately, it may be impractical to adapt anatomically-representative models for real-time clinical control applications, as an overwhelming number of parameters would need to be customized. Adjusting models parameters for amputees is even more challenging since (1) there is no intact musculoskeletal structure from which to measure parameters directly, and (2) the perceived biomechanical actions associated with EMG signals are not observable and may be altered from that of a healthy, intact limb due to cortical reorganization (Ramachandran and Hirstein, 1998). Measuring EMG for several muscles, especially deep muscles, may also be clinically challenging and subject to crosstalk. Finally, forward dynamic simulation of models with several musculoskeletal elements can be computationally intensive.

* Correspondence to: North Carolina State University, Campus Box 7115, Raleigh, NC 27695-7115. Fax: +1 919 515 7760.
E-mail address: dlcrouch@ncsu.edu (D.L. Crouch).

http://dx.doi.org/10.1016/j.jbiomech.2016.10.035
0021-9290/

As a counter to complex models, lumped-parameter models that combine the action of several muscles into fewer muscle elements may be more clinically practical (Eilenberg et al., 2010; Lehman and Calhoun, 1990; Messier et al., 2011). Modeling fewer muscle elements reduces (1) the number of parameters that must be adjusted for each subject, (2) the number of input EMG signals, and (3) the computational burden of forward dynamic simulation. To streamline the development of subject-specific models, researchers have used numerical optimization to adjust existing or define novel parameters to minimize error between measured and predicted joint *moments* given input EMG signals (Lehman and Calhoun, 1990; Lloyd and Buchanan, 1996; Shin et al., 2009). However, methods based on joint moments cannot be applied for amputees since the moments in the missing joints are indeterminable. Though both motion and force mirroring have been used as an indicator of amputee movement intent (Kamavuako et al., 2012; Muceli and Farina, 2012), force may not be truly mirrored since amputees cannot actively resist external loads on their amputated side. Therefore, we propose to compute a novel set of musculoskeletal parameters for a lumped-parameter model to match measured joint *kinematics*.

The objective of our pilot study was to develop and preliminarily test a lumped-parameter, 2 DOF model of the hand. Specifically, we wanted to (1) demonstrate that the model could reasonably predict joint kinematics during single-joint and simultaneous two-joint movements for able-bodied subjects and a transradial amputee; (2) compare the active and passive joint moment-generating capacity of subjects' models to that reported for healthy, intact limbs; and (3) evaluate the performance and repeatability of numerical optimization for computing model parameters. Our findings may promote the development and translation of real-time musculoskeletal model-based forward dynamic simulation for multifunctional upper limb prosthesis control.

2. Methods

2.1. Experiments and data collection

Experiments were approved by the institutional review board. Five able-bodied (AB1-AB5) subjects (3 males, 2 females, age range 23–31 years) and 1 subject (TRA) with transradial amputation (male, age 42) provided informed consent to participate. Subject TRA sustained a right traumatic amputation approximately 2 years before participating, and regularly used a body-powered prosthesis.

In one session, subjects performed 5 different types of movement in a static upper limb posture with the arm and forearm in neutral posture and elbow flexed to 90°: (1) wrist flexion/extension only, variable speed; (2) MCP flexion/extension only, variable speed; (3) simultaneous wrist and MCP flexion/extension, variable speed; (4) wrist flexion/extension only, fixed speed; and (5) MCP flexion/extension only, fixed speed. During *variable speed* movements, subjects moved in self-selected speeds and directions. In *fixed speed* trials, subjects alternated between maximum extension, relaxed, and maximum flexion joint postures at a regulated tempo (0.25 Hz). Able-bodied subjects performed the movements with the dominant arm, while subject TRA mirrored movements bilaterally. Each movement type was tested in two trials for at least 30 s; each subject performed a total of 10 trials (5 movements x 2 trials/movement). Subjects rested between trials.

During trials, EMG and kinematic data were collected synchronously from able-bodied subjects' dominant limb; for subject TRA, EMG and kinematics were measured from the residual and sound limb, respectively. Four bipolar surface EMG electrodes (Biometrics, Newport, UK) were placed over muscles/muscle groups (Fig. 1) identified by anatomical reference and palpation during experimenter-directed movements, and confirmed by visualizing EMG. The selected muscles generate wrist and metacarpophalangeal (MCP) flexion and extension joint moments in intact limbs based on their musculoskeletal geometry (Perotto, 2005). EMG data were sampled at 960 Hz, high-pass filtered at 40 Hz, rectified, enveloped, and low-pass filtered at 6 Hz using a 4th order Butterworth zero-phase filter, similar to previous methods (Lloyd and Besier, 2003). EMG were then normalized by respective maximum (post-processed) EMG signal values recorded during maximum voluntary contractions.

Given the short length of subject TRA's residual limb, EMG associated with wrist flexion appeared in electrodes targeting both wrist and MCP flexion, as flexor digitorum (MPC flexion) is deep to flexor carpi ulnaris (wrist flexion) in the proximal forearm. Therefore, similar to a previous method (Reddy and Gupta, 2007), we linearly transformed MCP flexor EMG ($EMG_{MCPflex}$)to reduce EMG associated with wrist flexion, based on the approximate proportion of wrist flexor EMG ($EMG_{wristflex}$) appearing in $EMG_{MCPflex}$ during isolated wrist flexion movements (Eq.1):

$$EMG^{*}_{MCPflex} = EMG_{MCPflex} - 0.75 EMG_{wristflex} \tag{1}$$

Reflective markers were placed on 9 anatomical locations to track distal limb motion (Fig. 1); thumb motion was not recorded or included in the model. Three-dimensional marker positions were recorded at 120 Hz using an infrared motion capture system (Vicon Motion Systems Ltd., UK), and filtered at 6 Hz using a 4th order Butterworth filter. Wrist and MCP joint angles were computed from filtered marker data using a musculoskeletal model (Holzbaur et al., 2005a) in OpenSim (Delp et al., 2007) that was modified to include the 2nd through 5th MCP joints.

2.2. Dynamic hand model

We defined a planar link-segment dynamic model (dynamic properties described in Supplementary Data) with two degrees of freedom (DOFs) - wrist and MCP flexion/extension – that was encoded in MATLAB (MathWorks, Inc., Natick, MA). Four muscles, one for each EMG source, were represented as Hill-type actuators with a contractile element (*CE*) and parallel elastic element (*PEE*) (Winters, 1990). A series elastic element, commonly included in Hill-type models to represent tendon, was not included. The force output of the contractile element, F^{CE}, was a function of its length (L^{CE}), shortening velocity (v^{CE}), and state of activation (a) (Eq. 2).

$$F^{CE} = f(L^{CE}) f(v^{CE}) a \tag{2}$$

where $f(L^{CE})$ is the active *CE* force (Eq. 3) and $f(v^{CE})$ is a hyperbolic scaling function that reduces F^{CE} as v^{CE} increases (Eq. 4).

$$f(L_{CE}) = F_0^{CE}\left(1 - \frac{(L^{CE} - L_0^{CE})^2}{W^2 (L_0^{CE})^2}\right) \qquad f(L^{CE}) > 0.01 \tag{3}$$

$$f(v_{CE}) = \frac{v_{max}^{CE} - v^{CE}}{v_{max}^{CE} + (\frac{v^{CE}}{c})} \qquad 0 < f(v^{CE}) < 1 \tag{4}$$

In Eq. 3, L_0^{CE} is the optimal *CE* length, and w, which defined the range over which the *CE* could produce force as a fraction of L_0^{CE}, was set at 0.5 (Buchanan et al., 2004). In Eq. 4 the maximum *CE* shortening velocity (v_{max}^{CE}) was set to 10 $\frac{L_0^{CE}}{s}$, and the hyperbolic shape factor (c) was set to 0.25 (Winters, 1990; Zajac, 1989). The parallel elastic element generated force (F^{PEE}) when its length exceeded L_0^{CE} (Eq. 5).

$$F^{PEE} = K^{PEE}(L^{CE} - L_0^{CE})^2 \qquad L^{CE} > L_0^{CE} \tag{5}$$

Muscle activation states, ranging between 0 (inactive) and 1 (fully activated), were computed from EMG, accounting for the electromechanical delay between neural excitation, represented by EMG, and muscle force production (Lloyd and Besier, 2003). Net joint moments (M_j) at joint j were computed as the product of muscle force and moment arm (ma) for each muscle n, summed across all k muscles (k=4 in our model) (Eq. 6).

$$M_j = \sum_{n=1}^{k} F_n^{CE} \times ma(n)_j \tag{6}$$

ma was assumed constant with respect to joint angle. Joint moments were applied during a forward dynamic simulation. Joint kinematics were computed by numerically integrating the equations of motion over 1/120 second time intervals using a 4th order Runge–Kutta method (Chadwick et al., 2009).

2.3. Numerical optimization

Twenty-two musculoskeletal parameters, constrained to approximate physiologic ranges (Holzbaur et al., 2005b), were computed by constrained global numerical optimization. Six parameters were computed for each muscle (Table 1), except, for wrist flexor and extensor muscles that only crossed the wrist and had no moment arm at the MCP joint,ma_{MCP} was set to zero. These parameters were chosen because they strongly influence the force- and moment-generating behavior of muscle.

For each subject, data from 5 of the 10 trials, one selected arbitrarily from each of the five movement types, were used for optimization. In each optimization loop, muscle activations were control inputs during a forward dynamic simulation. Since the range of motion of the wrist is greater than that of the MCP joint (Norkin and White, 2009), musculoskeletal parameters were optimized in order to minimize the

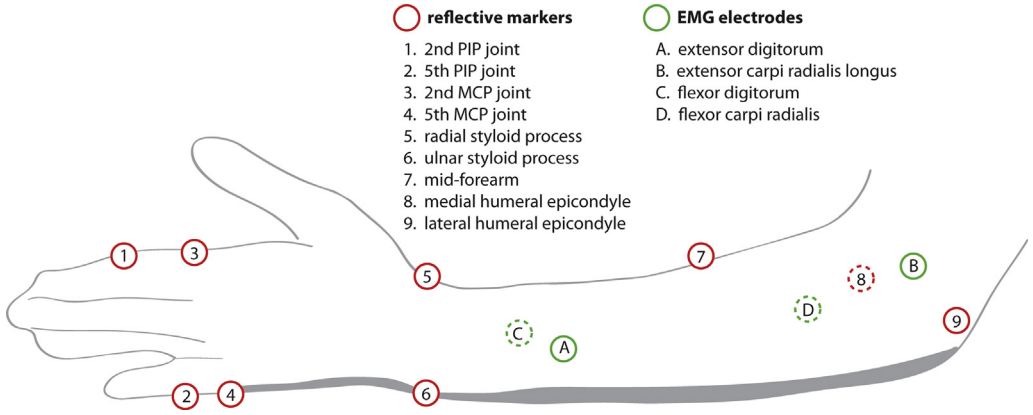

Fig. 1. EMG electrode and reflective marker placement for EMG and kinematic data recording, respectively. Illustration shows the anterior aspect of the forearm. Dotted circles indicate marker/electrode located on the anterior aspect of the forearm. PIP=proximal interphalangeal; MCP=metacarpophalangeal.

Table 1
Musculoskeletal parameter constraints during optimization.

Parameter (units)	Constraint
Optimal contractile element length (m)	$0.01 \le L_0^{CE} \le 0.5$
Maximum isometric contractile element force (N)	$10 \le F_0^{CE} \le 1000$
Moment arm, wrist (m)	$0.001 \le ma_{wrist} \le 0.05$
Moment arm, MCP* (m)	$0.001 \le ma_{MCP} \le 0.05$
Contractile element length in neutral posture (unitless)	$0.75L_0^{CE} \le L_{\theta=0}^{CE} \le 1.25L_0^{CE}$
Passive elastic element stiffness (N/m^2)	$10 \le K^{PEE} \le 200$

*$ma_{MCP}=0$ for wrist flexor/extensor muscles.

Table 2
Optimization algorithm parameters defined for Matlab's *GlobalSearch* function and simulated annealing.

GlobalSearch			**Simulated annealing**	
Fmincon	"MaxIter"	8000	Cooling rate (%)	10
Solver	"MaxFunEvals"	8000	Number of cooling cycles	20
Settings	"TolFun"	0.01	Number of searches in each cycle	10,000
GlobalSerch settings	"NumTrialPoints"	700		

weighted (MCP weight = 2 x wrist weight) sum of squared differences between measured and predicted kinematics. Parameters were optimized for each individual subject using MATLAB's *GlobalSearch* function. For comparison, we optimized parameters for a randomly-selected able-bodied subject by simulated annealing (SA), a widely used technique for solving complex, non-linear biomechanical optimization problems (Higginson et al., 2005). Optimization settings are shown in Table 2.

2.4. Data analysis

We estimated how well the model predicted subjects' wrist and MCP joint angles using a cross validation approach. We computed Pearson's correlation coefficient (r) between measured and predicted angles over a contiguous 25-second time window for variable speed trials not included in the optimization procedure. We also reported the strength of correlation (e.g. high, very high) based on a previously established scale (Hinkle et al., 2003). For subject TRA, model-predicted kinematics were compared to measured sound limb kinematics.

As further validation, we compared the passive and maximum isometric (passive+active) joint moments that subjects' models could generate (scaled to account for higher hand mass) with reported experimental values (Delp et al., 1996; Knutson et al., 2000; Mathiowetz et al., 1985) using a Welch's *t*-test for independent samples. Passive and maximum isometric wrist joint moments were computed with the MCP joint in neutral posture. Passive MCP joint moments were computed with the wrist in neutral posture. Maximum isometric MCP flexion moments were computed with the wrist in neutral posture and MCP in 45° flexion to approximate subjects' posture during grip strength tests (Mathiowetz et al., 1985).

Finally, we compared optimization results from *GlobalSearch* and SA algorithms. To assess optimization consistency, we executed 10 optimization routines with both *GlobalSearch* and SA algorithms for the aforementioned randomly-selected able-bodied subject. A paired Student's t-test was performed to compare prediction accuracy between *GlobalSearch* and SA (as measured by Pearson's correlation coefficient). Statistical differences were considered significant for $p < 0.05$.

3. Results

Models with *GlobalSearch*-computed parameters (Table 3) reasonably predicted able-bodied subjects' wrist and MCP joint kinematics, even during simultaneous wrist-MCP joint movement (Fig. 2 and Supplementary Data). For subject TRA, kinematic predictions driven by EMG measured from the residual limb matched the relative magnitude and direction of joint movement measured from the sound limb (Fig. 3), though not as well as for able-bodied subjects. Offline, the model could execute an EMG-driven forward dynamic simulation of a 20-second trial in approximately 1.5 s, demonstrating that the model permits simulation speeds required for real-time control.

The model's joint angle predictions showed high (0.7–0.9) to very high (> 0.9) positive correlation ($p < 0.001$ for all correlations) with measured joint angles across nearly all trials (Fig. 4). Across able-bodied subjects, mean correlation coefficient (r) values during wrist-only and MCP-only movements at those joints were 0.94 (SD=0.02) and 0.88 (SD=0.02), respectively. Similarly, correlations for subject TRA were very high at both the wrist ($r=0.92$) and MCP ($r=0.93$) joints when they were moved independently. During simultaneous wrist-MCP movement, mean correlations across able-bodied subjects remained high at both the wrist (mean $r=0.89$, SD=0.04) and MCP (mean $r=0.75$, SD=0.06) joints. For the same movement, subject TRA's predicted and measured kinematics were very highly correlated at the wrist ($r=0.93$), but moderately correlated at the MCP joint ($r=0.56$).

The model's force-generating behavior was generally consistent with that of healthy adults. Model-generated absolute passive moments were slightly, but not significantly, higher at the extremes of joint range of motion compared to experimental measurements; however, as in the biological limb, the joints were statically stable since passive forces tended to return joints to neutral posture (Fig. 5). Likewise, the maximum isometric joint moments generated by the model were not significantly different from physiologic values (Fig. 6).

Table 3
Optimized musculoskeletal parameters for the four virtual muscles for all subjects (L_0^{CE} = optimal muscle length (m), F_0^{CE} = maximum isometric muscle force (N), ma = moment arm (m), $L_{\theta=0}^{CE}$ = muscle length in neutral posture (m), K^{PEE} = parallel elastic element stiffness (N/m^2)).

Subject	Parameter	Virtual muscle			
		Wrist extensor	MCP extensor	Wrist flexor	MCP flexor
AB1	L_0^{CE}	0.238	0.054	0.109	0.179
	F_0^{CE}	1000	42	234	257
	ma_{wrist}	−0.050	−0.013	0.050	0.050
	ma_{MCP}	0	−0.050	0	0.050
	$L_{\theta=0}^{CE}$	1.109	0.750	1.153	1.122
	K^{PEE}	53	22	160	54
AB2	L_0^{CE}	0.257	0.071	0.133	0.026
	F_0^{CE}	332	59	530	265
	ma_{wrist}	−0.049	−0.029	0.041	0.004
	ma_{MCP}	0	−0.034	0	0.018
	$L_{\theta=0}^{CE}$	1.130	1.033	1.046	1.250
	K^{PEE}	149	25	182	67
AB3	L_0^{CE}	0.150	0.171	0.412	0.146
	F_0^{CE}	366	80	651	316
	ma_{wrist}	−0.050	−0.028	0.050	0.038
	ma_{MCP}	0	−0.050	0	0.050
	$L_{\theta=0}^{CE}$	1.225	1.016	1.197	1.130
	K^{PEE}	200	200	200	75
AB4	L_0^{CE}	0.239	0.039	0.250	0.442
	F_0^{CE}	584	130	261	99
	ma_{wrist}	−0.050	−0.019	0.049	0.025
	ma_{MCP}	0	−0.038	0	0.049
	$L_{\theta=0}^{CE}$	1.032	0.762	1.023	1.161
	K^{PEE}	200	10	194	196
AB5	L_0^{CE}	0.022	0.012	0.500	0.047
	F_0^{CE}	1000	272	906	108
	ma_{wrist}	−0.015	−0.005	0.013	0.017
	ma_{MCP}	0	−0.012	0	0.032
	$L_{\theta=0}^{CE}$	1.182	1.241	1.208	1.250
	K^{PEE}	149	10	136	101
TRA	L_0^{CE}	0.078	0.019	0.070	0.183
	F_0^{CE}	256	42	107	56
	ma_{wrist}	−0.029	−0.001	0.031	0.050
	ma_{MCP}	0	−0.015	0	0.016
	L_0^{CE}	1.125	0.776	0.857	0.968
	K^{PEE}	10	118	97	200

For randomly-selected subject AB4, ten repeated *GlobalSearch* optimization routines yielded a model with very consistent predictive capability. The mean and standard deviation of correlation coefficient between measured and predicted joint angles were 0.92 (SD = 0.004) and 0.71 (SD = 0.05) at the wrist and MCP joints, respectively (Fig. 7). Variation in correlation coefficient was greater when parameters were computed by simulated annealing (mean $r = 0.93$, SD = 0.006 and mean $r = 0.52$, SD = 0.13 at the wrist and MCP joints, respectively). Correlation coefficient at the wrist was only 0.01 greater for SA ($p < 0.001$), while correlation coefficient at the MCP joint was 0.19 lower for SA ($p < 0.001$). Both *GlobalSearch* and simulated annealing took approximately 20 h to execute on a desktop computer (Dell Precision T5810, 3.70 GHz processor, 32 GB RAM).

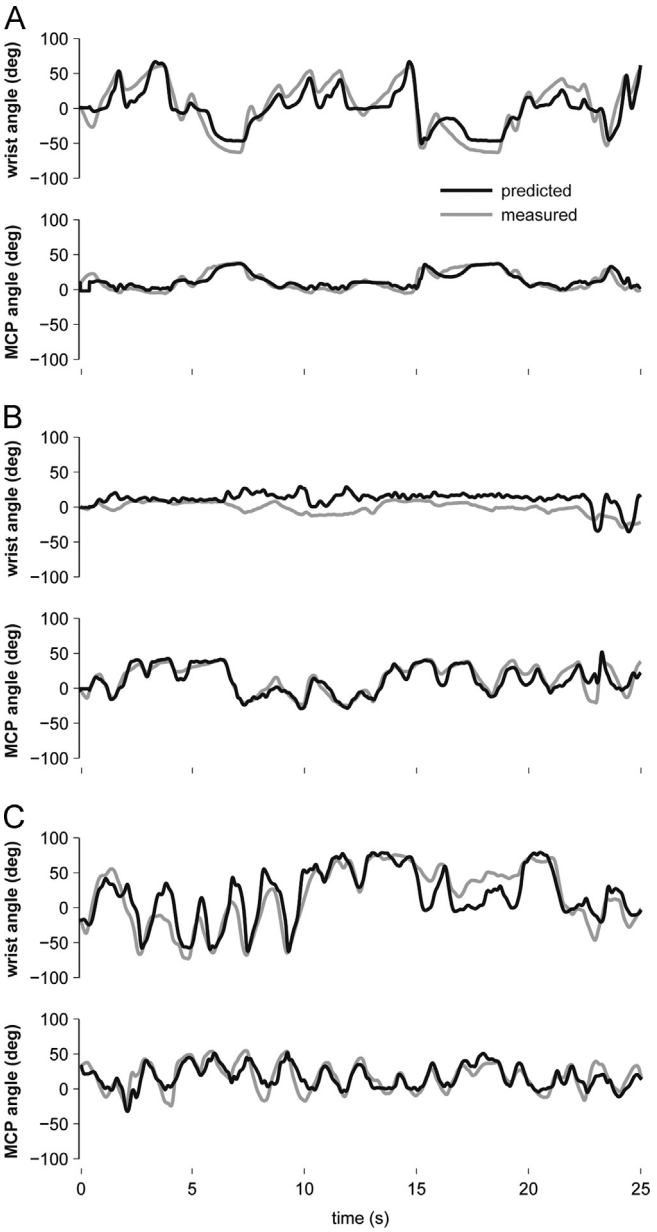

Fig. 2. Measured and predicted wrist and MCP joint angles during (A) wrist-only, (B) MCP-only, and (C) simultaneous wrist and MCP varying speed movements from subject AB5.

4. Discussion

We demonstrated that a simple, lumped-parameter, EMG-driven musculoskeletal model of the wrist and hand could reasonably predict both single-joint and multi-joint wrist and MCP movements for both able-bodied and amputee subjects. As further validation, we found that the passive and maximum isometric joint moment-generating capacity of the model approximated that of healthy adults. Model predictions of sub-maximal kinematics were more accurate than passive and maximal active kinetic predictions, which was not surprising since the model parameters were computed using experimental sub-maximal kinematic data. However, it was notable that the model mimicked the passive static stability and approximate maximum isometric strength of the human hand, though it had substantially fewer muscles than the biological limb.

For clinical applications, an optimization approach may be better suited for defining model parameters than conventional

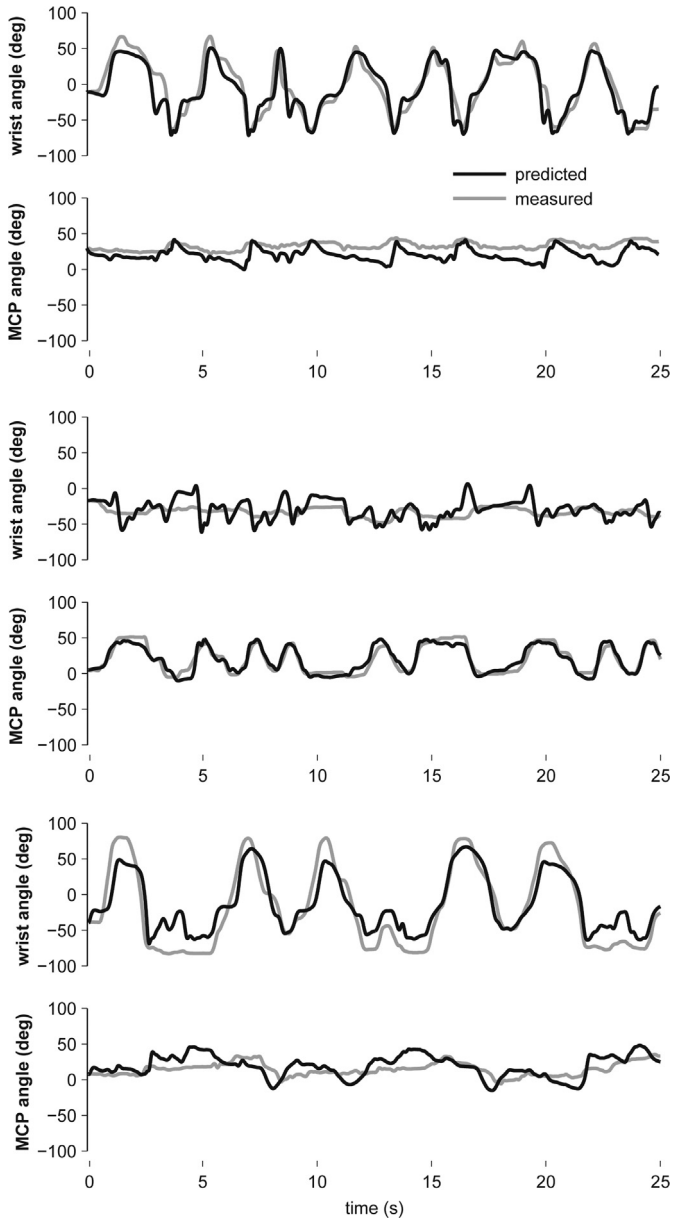

Fig. 3. Measured and predicted wrist and MCP joint angles during (A) wrist-only, (B) MCP-only, and (C) simultaneous wrist and MCP varying speed movements from subject TRA.

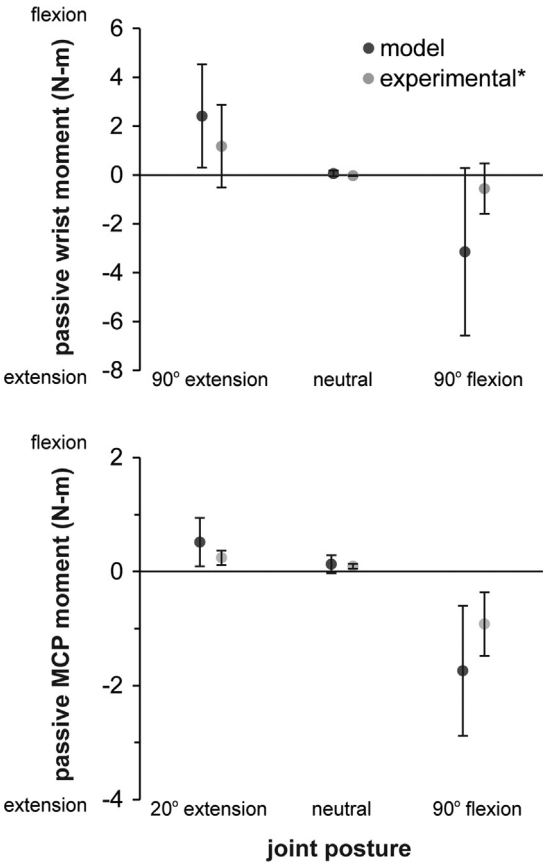

Fig. 5. Mean model-predicted and experimentally-measured passive flexion, extension, and neutral joint moments at the wrist (top) and MCP (bottom) joints. Bars indicate ±standard deviation.

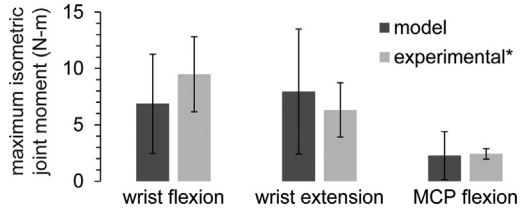

Fig. 6. Mean model-predicted and experimentally-measured maximum isometric joint moments at the wrist (neutral posture) and MCP (45° flexion) joints. MCP extension moments were excluded because experimental data were not available. *Experimental wrist data adapted from (Delp et al., 1996), and MCP data adapted from (Mathiowetz, et al. 1985). MCP joint moment was computed from linear force data from the right hand of 20–24 year old males assuming a 2 cm moment arm between the dynamometer handle and MCP joint.

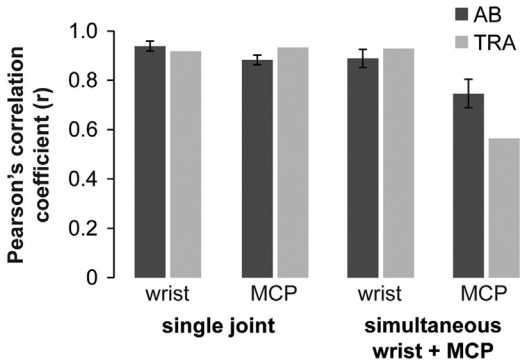

Fig. 4. Pearson's correlation coefficient (r) between measured and predicted joint angles during single-joint and simultaneous multi-joint (wirst and MCP) movements.

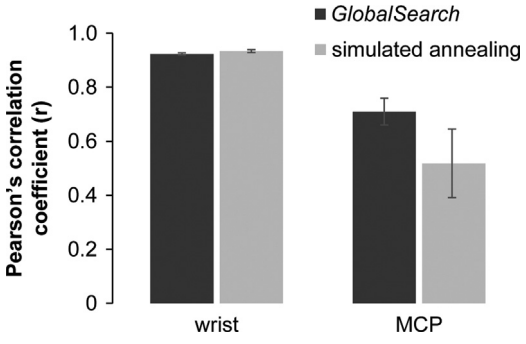

Fig. 7. Correlation between measured and predicted joint angles during simultaneous wrist-MCP movement when musculoskeletal parameter values were computed either by Matlab's *GlobalSearch* function or simulated annealing ($n=10$ routines with each algorithm) for subject AB4.

methods based on direct anatomical measurements. Common sources of anatomical data include musculoskeletal specimens (Lieber et al., 1992; Murray et al., 1995), medical imaging (Holzbaur et al., 2007), or functional strength tests (Lehman and Calhoun, 1990). Such sources may be inappropriate for defining parameters in a lumped-parameter model whose muscles have no direct anatomical analog, and for amputees whose muscles no longer span the missing limb. However, if prediction accuracy is not compromised, defining values for some model parameters, such as moment arm, using experimental data may further simplify our modeling approach.

Despite searching over a relatively large set of 22 parameters, Matlab's *GlobalSearch* optimization algorithm, a gradient-based method, yielded better predictions than simulated annealing (SA), a stochastic method. However, other algorithms may search more efficiently and extensively over the parameter space. For instance, simulated annealing parallelized across multiple processors can test several points simultaneously (Higginson et al., 2005). Simplifying the optimization problem by reducing the number of optimized parameters, shortening the simulation in each iteration, obtaining prior knowledge, or further constraining parameter values may also improve efficiency. Sensitivity analyses are needed to identify appropriate simplifications that do not diminish optimization performance or prediction accuracy.

Several amputees, including our subject TRA, experience phantom limb sensations with voluntary muscle contraction (Ramachandran and Hirstein, 1998). This suggest that amputees retain an internal representation of their missing limb that may allow them to generate functionally-relevant motor commands after amputation (Mercier et al., 2006; Wolpert and Flanagan, 2001). That motor commands retain functional meaning is further evidenced in the ability of machine learning algorithms to distinguish among several different intended motions from multichannel EMG (Li et al., 2010; Zhang and Huang, 2015). However, few have investigated the implicit, perceived biomechanical actions of individual residual muscles following amputation. That we could predict independent flexion and extension motion of the wrist and MCP joints for subject TRA suggests that amputees' residual muscles may retain unique functional roles that can be coordinated across several muscles to produce intentional multijoint movements. By capturing the perceived biomechanical structure of an amputees missing limb, our model could help researchers further investigate these implicit functional roles to improve myoelectric prosthesis control.

MCP joint angle prediction accuracy (as quantified by Pearson's correlation coefficient) was lower across subjects during multijoint movements than during single-joint movements, especially for subject TRA. This may have been due to greater EMG crosstalk, a known limitation of surface electromyography, during MCP movement when the wrist was moved simultaneously. Additionally, EMG electrodes may have been placed imprecisely. Potential approaches and tools to acquire localized EMG signals include intramuscular EMG recording (Riek et al., 2000; Weir et al., 2009), spatial filters applied to high-density recordings (Huang et al., 2009), or medical imaging (Boon et al., 2011). Muscle loss, reduced somatosensory feedback, and motor reorganization may also influence the quality and accessibility of EMG recordings from amputees. These challenges have been addressed by emerging technologies, such as targeted nerve reinnervation to reaccess neuromuscular control signals to the missing limbs (Kuiken et al., 2009) and nerve stimulation to restore natural sensation (Tan et al., 2014). Our model may benefit from these technologies and, in turn, accurately estimate amputee movement intent in a novel way to advance multifunctional prosthesis control and restore functional motor coordination patterns in amputees. Combining our model with these advanced neural technologies will be interesting future work.

4.1. Limitations

The study included relatively few subjects, including only one individual with transradial amputation, so it is unclear whether the model performance would be consistent across the clinical population. With further development, we plan to evaluate the model's offline and real-time performance for more subjects to more broadly characterize its clinical viability as a prosthesis control platform.

Several simplifying assumptions, some of which are discussed below, were made to design a model that would be practical for prosthesis control, as a more complex model may increase computation time and the number of parameter values to compute or estimate.

1. We did not include tendons, which store elastic energy and transmit force from muscles in the forearm to the joints of the wrist and hand, allowing much of the muscle mass contributing to hand function to be located proximally. For a given muscle-tendon length, tendon reduces the excursion of the CE so that, through a given range of joint rotation, the CE operates over a smaller portion of the force-length curve. This effect of tendon on muscle-tendon mechanics could be somewhat replicated in our model by a CE only with a longer optimal length. Accounting for musculotendon dynamics would require additional computational resources, making real-time prosthesis control more challenging to achieve.
2. Muscle moment arms were assumed constant with respect to joint angle. Some muscles (e.g. flexor carpi radialis, extensor digitorum) that cross the wrist and MCP joints have relatively constant moment arms, while others (e.g. extensor carpi radialis longus, flexor digitorum superficialis) do not (An et al., 1983; Gonzalez et al., 1997).
3. Only four muscles were included in the model, though there are over 40 muscles that may contribute to wrist and hand movement (Jacobson et al., 1992; Keir et al., 1996).
4. The model represented wrist and finger motion, but did not include a thumb, which is critical for grasping objects. Myoelectric prostheses typically do not enable explicit control of thumb motion, but rather include it implicitly in the design and functionality. For instance, a prosthetic thumb mechanism opposing the fingers can be fixed or commanded to flex when the finger mechanism flexes (i.e. finger flexion in our model) to enable grasp.

Our simplification of the hand likely contributed to kinematic prediction errors. Whether the model enables effective real-time control despite prediction errors will be the focus of future studies.

4.2. Conclusion

In conclusion, our musculoskeletal model yielded reasonably accurate predictions of single-joint and simultaneous multi-joint movements. The model's simplified structure and optimization-derived parameters make it more practical to adapt to clinical populations while still mimicking the dynamic behavior of the biological limb. Though primarily intended as a clinical tool for real-time prosthesis control, the model may be useful for investigating neuromuscular control and adaptation in healthy and impaired individuals.

Conflict of interest

The authors declare that there are no conflicts of interest to disclose.

Acknowledgements

This work was sponsored by Defense Advanced Research Projects Agency (DARPA) Biological Technologies Office (BTO) Hand Proprioception and Touch Interfaces (HAPTIX) program under the auspices of Dr. Doug Weber through the DARPA Contracts Management Office Grant/Contract no. N66001-16-2-4052.This project was also supported by NSF #1527202, DHHS/NIDILRR #90IF0064, and DOD #OR140147 & #13014002. We thank Lewis Gaffney for assisting with data collection.

Appendix A. Supporting information

Supplementary data associated with this article can be found in the online version at http://dx.doi.org/10.1016/j.jbiomech.2016.10.035.

References

An, K.N., Ueba, Y., Chao, E.Y., Cooney, W.P., Linscheid, R.L., 1983. Tendon excursion and moment arm of index finger muscles. J. Biomech. 16, 419–425.
Boon, A.J., Oney-Marlow, T.M., Murthy, N.S., Harper, C.M., McNamara, T.R., Smith, J., 2011. Accuracy of electromyography needle placement in cadavers: non-guided vs. ultrasound guided. Muscle Nerve 44, 45–49.
Buchanan, T.S., Lloyd, D.G., Manal, K., Besier, T.F., 2004. Neuromusculoskeletal modeling: estimation of muscle forces and joint moments and movements from measurements of neural command. J. Appl. Biomech. 20, 367–395.
Chadwick, E.K., Blana, D., van den Bogert, A.J., Kirsch, R.F., 2009. A real-time, 3-D musculoskeletal model for dynamic simulation of arm movements. IEEE Trans. Biomed. Eng. 56, 941–948.
Delp, S.L., Anderson, F.C., Arnold, A.S., Loan, P., Habib, A., John, C.T., Guendelman, E., Thelen, D.G., 2007. OpenSim: open-source software to create and analyze dynamic simulations of movement. IEEE Trans. Biomed. Eng. 54, 1940–1950.
Delp, S.L., Grierson, A.E., Buchanan, T.S., 1996. Maximum isometric moments generated by the wrist muscles in flexion-extension and radial-ulnar deviation. J. Biomech. 29, 1371–1375.
Delp, S.L., Loan, J.P., Hoy, M.G., Zajac, F.E., Topp, E.L., Rosen, J.M., 1990. An interactive graphics-based model of the lower extremity to study orthopaedic surgical procedures. IEEE Trans. Biomed. Eng. 37, 757–767.
Eilenberg, M.F., Geyer, H., Herr, H., 2010. Control of a powered ankle-foot prosthesis based on a neuromuscular model. IEEE Trans. Neural Syst. Rehabil. Eng. 18, 164–173.
Gonzalez, R.V., Buchanan, T.S., Delp, S.L., 1997. How muscle architecture and moment arms affect wrist flexion-extension moments. J. Biomech. 30, 705–712.
Higginson, J.S., Neptune, R.R., Anderson, F.C., 2005. Simulated parallel annealing within a neighborhood for optimization of biomechanical systems. J. Biomech. 38, 1938–1942.
Higginson, J.S., Zajac, F.E., Neptune, R.R., Kautz, S.A., Delp, S.L., 2006. Muscle contributions to support during gait in an individual with post-stroke hemiparesis. J. Biomech. 39, 1769–1777.
Hinkle, D., Wiersma, W., Jurs, S., 2003. Applied Statistics for the Behavioral Sciences, 5 ed. Houghton Mifflin, Boston.
Holzbaur, K.R., Murray, W.M., Delp, S.L., 2005a. A model of the upper extremity for simulating musculoskeletal surgery and analyzing neuromuscular control. Ann. Biomed. Eng. 33, 829–840.
Holzbaur, K.R.S., Murray, W.M., Delp, S.L., 2005b. A model of the upper extremity for simulating musculoskeletal surgery and analyzing neuromuscular control. Ann. Biomed. Eng. 33, 829–840.
Holzbaur, K.R.S., Murray, W.M., Gold, G.E., Delp, S.L., 2007. Upper limb muscle volumes in adult subjects. J. Biomech. 40, 742–749.
Huang, H., Zhou, P., Li, G., Kuiken, T., 2009. Spatial filtering improves EMG classification accuracy following targeted muscle reinnervation. Ann. Biomed. Eng. 37, 1849–1857.
Jacobson, M.D., Raab, R., Fazeli, B.M., Abrams, R.A., Botte, M.J., Lieber, R.L., 1992. Architectural design of the human intrinsic hand muscles. J. Hand Surg. 17, 804–809.
Kamavuako, E.N., Farina, D., Yoshida, K., Jensen, W., 2012. Estimation of grasping force from features of intramuscular EMG signals with mirrored bilateral training. Ann. Biomed. Eng. 40, 648–656.
Keir, P.J., Wells, R.P., Ranney, D.A., 1996. Passive properties of the forearm musculature with reference to hand and finger postures. Clin. Biomech. (Bristol, Avon) 11, 401–409.
Knutson, J.S., Kilgore, K.L., Mansour, J.M., Crago, P.E., 2000. Intrinsic and extrinsic contributions to the passive moment at the metacarpophalangeal joint. J. Biomech. 33, 1675–1681.
Kuiken, T.A., Li, G., Lock, B.A., Lipschutz, R.D., Miller, L.A., Stubblefield, K.A., Englehart, K.B., 2009. Targeted muscle reinnervation for real-time myoelectric control of multifunction artificial arms. J. Am. Med. Assoc. 301, 619–628.
Lehman, S.L., Calhoun, B.M., 1990. An identified model for human wrist movements. Exp. Brain Res. 81, 199–208.
Li, G., Schultz, A.E., Kuiken, T.A., 2010. Quantifying pattern recognition-based myoelectric control of multifunctional transradial prostheses. IEEE Trans. Neural Syst. Rehabil. Eng. 18, 185–192.
Lieber, R.L., Jacobson, M.D., Fazeli, B.M., Abrams, R.A., Botte, M.J., 1992. Architecture of selected muscles of the arm and forearm: anatomy and implications for tendon transfer. J. Hand Surg. 17, 787–798.
Lloyd, D.G., Besier, T.F., 2003. An EMG-driven musculoskeletal model to estimate muscle forces and knee joint moments in vivo. J. Biomech. 36, 765–776.
Lloyd, D.G., Buchanan, T.S., 1996. A model of load sharing between muscles and soft tissues at the human knee during static tasks. J. Biomech. Eng. 118, 367–376.
Manal, K., Buchanan, T.S., 2013. An electromyogram-driven musculoskeletal model of the knee to predict in vivo joint contact forces during normal and novel gait patterns. J. Biomech. Eng. 135, 021014.
Manal, K., Gonzalez, R.V., Lloyd, D.G., Buchanan, T.S., 2002. A real-time EMG-driven virtual arm. Comput. Biol. Med. 32, 25–36.
Mathiowetz, V., Kashman, N., Volland, G., Weber, K., Dowe, M., Rogers, S., 1985. Grip and pinch strength: normative data for adults. Arch. Phys. Med. Rehabil. 66, 69–74.
Mercier, C., Reilly, K.T., Vargas, C.D., Aballea, A., Sirigu, A., 2006. Mapping phantom movement representations in the motor cortex of amputees. Brain 129, 2202–2210.
Messier, S.P., Legault, C., Loeser, R.F., Van Arsdale, S.J., Davis, C., Ettinger, W.H., DeVita, P., 2011. Does high weight loss in older adults with knee osteoarthritis affect bone-on-bone joint loads and muscle forces during walking? Osteoarthr. Cartil. 19, 272–280.
Muceli, S., Farina, D., 2012. Simultaneous and proportional estimation of hand kinematics from EMG during mirrored movements at multiple degrees-of-freedom. IEEE Trans. Neural Syst. Rehabil. Eng. 20, 371–378.
Murray, W.M., Delp, S.L., Buchanan, T.S., 1995. Variation of muscle moment arms with elbow and forearm position. J. Biomech. 28, 513–525.
Neptune, R.R., Kautz, S.A., Zajac, F.E., 2001. Contributions of the individual ankle plantar flexors to support, forward progression and swing initiation during walking. J. Biomech. 34, 1387–1398.
Norkin, C.C., White, D.J., 2009. Measurement of joint motion: a guide to goniometry, 4th ed. F.A. Davis, Philadelphia.
Perotto, A.O., 2005. Anatomical guide for the electromyographer: the limbs and trunk, 4th ed. Charles C. Thomas Publisher, Ltd, Springfield, IL.
Ramachandran, V.S., Hirstein, W., 1998. The perception of phantom limbs. The D. O. Hebb lecture. Brain 121 (9), 1603–1630.
Reddy, N.P., Gupta, V., 2007. Toward direct biocontrol using surface EMG signals: control of finger and wrist joint models. Med. Eng. Phys. 29, 398–403.
Riek, S., Carson, R.G., Wright, A., 2000. A new technique for the selective recording of extensor carpi radialis longus and brevis EMG. J. Electromyogr. Kinesiol. 10, 249–253.
Saul, K.R., Murray, W.M., Hentz, V.R., Delp, S.L., 2003. Biomechanics of the Steindler flexorplasty surgery: a computer simulation study. J. Hand Surg. 28A, 979–986.
Shelburne, K.B., Pandy, M.G., 1998. Determinants of cruciate-ligament loading during rehabilitation exercises. Clin. Biomech. 13, 403–413.
Shin, D., Kim, J., Koike, Y., 2009. A myokinetic arm model for estimating joint torque and stiffness from EMG signals during maintained posture. J. Neurophysiol. 101, 387–401.
Tan, D.W., Schiefer, M.A., Keith, M.W., Anderson, J.R., Tyler, J., Tyler, D.J., 2014. A neural interface provides long-term stable natural touch perception. Sci. Transl. Med. 6 [257ra138].
Weir, R.F., Troyk, P.R., DeMichele, G.A., Kerns, D.A., Schorsch, J.F., Maas, H., 2009. Implantable myoelectric sensors (IMESs) for intramuscular electromyogram recording. IEEE Trans. Biomed. Eng. 56, 159–171.
Winters, J.M., 1990. Hill-based muscle models: a systems engineering. In: Winters, J.M., Woo, S.L.-Y. (Eds.), Perspective. Multiple Muscle SystemsSpringer-Verlag, New York, pp. 69–93.
Wolpert, D.M., Flanagan, J.R., 2001. Motor prediction. Curr. Biol. 11, R729–R732.
Zajac, F.E., 1989. Muscle and tendon: properties, models, scaling, and application to biomechanics and motor control. Crit. Rev. Biomed. Eng. 17, 359–411.
Zajac, F.E., Neptune, R.R., Kautz, S.A., 2002. Biomechanics and muscle coordination of human walking. Part I: introduction to concepts, power transfer, dynamics and simulations. Gait Posture 16, 215–232.
Zhang, X., Huang, H., 2015. A real-time, practical sensor fault-tolerant module for robust EMG pattern recognition. J. Neuroeng. Rehabil. 12, 18.